PACS numbers: 32.30.Rj; 41.50.+h; 52.25.Nr; 52.50.Jm
DOI: 10.1070/QE2000v030n08ABEH001798

X-ray emission spectra of the plasma produced by an ultrashort laser pulse in cluster targets

C Stenz, V Bagnoud, F Blasco, J R Roche, F Salin,
A Ya Faenov, A I Magunov, T A Pikuz,I Yu Skobelev

Abstract. The first observation of x-ray emission spectra of multiply charged ions in the plasma produced by a 35-fs laser pulse with an intensity up to 10^{17} W cm^{-2} in CO_2 and Kr gas jet targets is reported. The emission in the wavelength ranges of the $1snp - 1s^2 (n = 3 - 6)$ transitions of O VII ions and the Ly_α line of O VIII ions, as well as of the $(2s_{1/2}2p^6\,3p_{3/2})_1 - 2s^2 2p^6\,{}^1S_0$ and $(2s_{1/2}2p^6 3p_{1/2})_1 - 2s^2 2p^6\,{}^1S_0$ lines of Ne-like KrXXVII ions testifies that the highly ionised plasma is formed by collision processes in clusters. Modelling the shape of the spectral lines of oxygen ions by including the principal mechanisms of broadening and absorption in optically dense plasmas reveals that the main contribution to the time-integrated intensity is made by the plasma with the parameters $N_e = (2 - 20) \times 10^{20}$ cm^{-3} and $T_e = 100 - 115$ eV.

1. Introduction

Extensive investigations of the plasma produced by ultrashort laser pulses exceeding 1 TW in power are currently underway. Experiments are staged using both solid and gas targets. In the latter case, the investigations are concerned with phenomena like the generation of short-wavelength radiation, hot electrons, and fast ions, like self-focusing and channelling of the laser radiation, etc. [1 – 6]. These effects occur directly upon the interaction of the laser radiation with matter.

The specific features of plasma formation by an intense ultrashort laser pulse in gas targets reveal themselves in the plasma emission spectra following the passage of the pulse. For instance, complete ionisation of atoms in the light field of a laser pulse is accompanied by a rapid recombination with an amplification of the soft x-ray radiation at the resonance transition to the ground state of the H-like ion, which was observed in emission at 13.5 nm for the Ly_α transition in the LiIII ion [7]. The progress towards a shorter-wavelength spectral region is possible with targets of heavier elements. In a strongly supercooled plasma, recombination can proceed faster than radiative transitions from highly excited levels. This results in the formation of 'hollow' ions, in which all electrons reside in highly excited states and the emission spectrum in the vicinity of the corresponding resonance lines becomes quasi-continuous [8].

A study of gas targets with a high content of multiparticle clusters [9 – 11] is of special interest, because collision processes begin to play the dominant role in the plasma formation owing to a high atom density inside the clusters. At the same time, because of the relatively small size of the gas cluster, it is penetrated by the laser field, resulting in tunnel ionisation of the atoms. Recently, a significant thermonuclear neutron yield was detected upon photoionisation of deuterium-enriched cluster targets by an ultrashort laser pulse; the energies of the ions produced in the target were high enough for a fusion reaction to commence [12]. The study of the emission spectra of the plasma produced by ultrashort laser pulses yields additional information on the role of various processes in the plasma formation from clusters. In Ref. [13], the emission of multiply charged ions with the energy up to 1 MeV was detected.

In this paper, we used the x-ray spectroscopic techniques to study emission of the plasma produced by 35-fs laser pulses with an intensity up to 10^{17} W cm^{-2} in high-pressure gas jet targets of CO_2 and Kr, in which clusters are formed. The range of parameters of the plasma under study is determined by modelling the observed line spectra taking into account the principal mechanisms of line broadening.

2. Experimental

The experiments were performed at a laser setup at Bordeaux. Its operation involved a chirped-pulse amplification in a four-stage Ti:sapphire rod amplifier ($\lambda_L = 0.79$ μm) with subsequent reduction of the pulse length to 20 fs using diffraction gratings. The pumping was accomplished by the pulsed radiation from five Nd:YLF lasers with a repetition rate of 1 kHz, which allowed us to obtain output pulses with energies up to 20 mJ at the same repetition rate. A regenerative amplifier incorporated in the setup produced prepulses arriving a few nanoseconds prior to the main pulse. A Pockels cell was placed behind the first amplifier to suppress the prepulses and to augment the energy contrast ratio of the main pulse up to $10^4 - 10^5$. The background intensity was at least eight orders of magnitude lower than the pulse intensity.

A Ya Faenov, I Yu Skobelev Centre of Data on Multicharged-Ion Spectra Center of All-Russian Research Institute of Physicotechnical and Radio Engineering Measurements (VNIIFTRI), 141570 Mendeleevo, Moscow oblast, Russia; **C Stenz, V Bagnoud, F Blasco, J R Roche, F Salin** Centre Laser Intenses et Applications, Universite Bordeaux 1, 33405 Talence, France;
A I Magunov General Physics Institute, Russian Academy of Sciences, ul. Vavilova 38, 117942 Moscow, Russia;
T A Pikuz N E Bauman Moscow State Technical University, 2 Baumanskaya ul. 5, 107005 Moscow, Russia
Received 12 January 2000
Kvantovaya Elektronika **30** (8) 721 – 725 (2000)
Translated by E N Ragozin, edited by M N Sapozhnikov

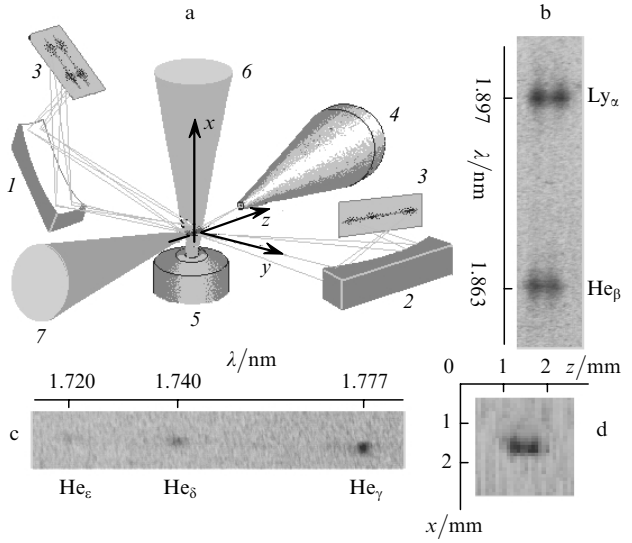

Figure 1. Schematic of the setup for measuring the x-ray emission spectra from a gas-target plasma (a); spectrogram of the spectrograph (*1*) having a spatial resolution along the laser beam axis (b); spectrogram of the spectrograph (*2*) with a spatial resolution across the laser beam axis (c); and pinhole camera x-ray plasma image (d): (*1, 2*) focusing spectrographs; (*3*) photographic film; (*4*) pinhole camera; (*5*) nozzle; (*6*) gas jet; (*7*) laser beam.

Provision was made for correcting the pulse front to ensure that the pulse length did not exceed 35 fs. As a precaution against damage to the compression gratings, the maximum pulse energy at the target did not exceed 15 mJ. The laser beam was focused by an off-axis parabolic mirror. The radius of the focal spot in vacuum was 6 μm at the $1/e^2$ level, which corresponds to a peak intensity of 10^{17} W cm^{-2}. The laser pulse was focused into the gas jet at a distance of 1.25 mm from the nozzle outlet.

The target was a pulsed gas jet (Fig. 1a) that was issued from a supersonic cylindrical nozzle 2.5 mm in diameter. The gas jet flew into the vacuum chamber with a velocity of 2.5 M and a divergence angle of 22°. The maximum gas pressure in the valve was 40 bar. Under these conditions, clusters are formed from Kr atoms [14] and CO_2 molecules [15] in the jet owing to Van der Waals forces. The maximum electron density in the clusters far exceeds the critical density $N_e^{cr} \approx 1.7{\cdot}10^{21}$ cm^{-3}. An indirect confirmation of the presence of clusters was that, with a prepulse which destroyed them (the electron tunneling from the outer atomic shell proceeds even at intensities of $10^{14} - 10^{15}$ W cm^{-2} [16]), the x-rays were absent.

The spatial characteristics of the resultant plasma were determined using a pinhole camera with a hole 10 μm in diameter. The image of the hot plasma region was recorded with a 2x magnification employing a CCD with 24 μm × 24 μm pixels. The CCD window was shielded with a filter made of a 2-μm-thick polypropylene layer coated on both sides by 0.2-μm-thick aluminium layers, which transmitted photons with energies above 200 eV. The viewing angle with respect to the laser beam axis was 20.5°, resulting in about a 40-μm spatial resolution in the axial direction.

The x-ray spectral measurements were carried out employing focusing spherical ($R = 150$ mm) mica crystal spectrographs [17] (Fig. 1a) in the $1.73 - 1.92$ nm (the first order of reflection) and $0.63 - 0.643$ nm (the third order of reflection) spectral ranges with the resolution $\lambda/\Delta\lambda \approx 2000$. The spectrographs were arranged to view the plasma at a right angle to the laser beam axis and ensured spatial resolution either along this axis or across it. The spectra were recorded on a RAR-2492 photographic film through a filter composed of a 2-μm-thick layer of polypropylene coated on either side by aluminium layers 0.4 μm in thickness.

3. Modelling of the spectra

A spectrograph records a time-integrated signal, corresponding to the emission in a narrow angular range, with a one-dimensional spatial resolution. At each instant in time, the plasma characteristics are nonuniform within the emitting region. In modelling the observed spectra, it was assumed that the radiation intensity is determined by the sum each term in which corresponds to the contribution of a uniform plasma region with a specific (average) temperature and electron density, as well as ionic-charge plasma composition:

$$I(\omega) = \sum_i C_i Q(\omega)[\varkappa(\omega)]^{-1}\{1 - \exp[-\varkappa(\omega)L_i]\}, \qquad (1)$$

where

$$Q(\omega) = \hbar\omega \sum_n A_{n1} S_{n1}(\omega) N_n + Q_{br}(\omega) + Q_{rec}(\omega) \qquad (2)$$

is the emissive power of the plasma (line, bremsstrahlung, and photorecombination radiation);

$$\varkappa(\omega) = \left(\frac{\pi c}{\omega}\right)^2 \sum_n g_n A_{n1} S_{n1}(\omega) \frac{N_1}{g_1} + \varkappa_{br}(\omega) + \varkappa_{ion}(\omega) \qquad (3)$$

is the resonance and nonresonance (inverse bremsstrahlung and photoionisation) spectral absorption coefficient; S_{n1} is the spectral function normalised to unity; N_n and g_n are the population and the statistical weight of the ion level n; L_i is the linear dimension of the i-th emitting plasma region; and C_i is the geometric factor, which also takes into account integration with respect to time. For an optically thin plasma, expression (1) takes the form

$$I(\omega) = \sum_i C_i Q(\omega) L_i. \qquad (4)$$

In the calculation of the profiles of the $1snp \to 1s^2$ ($n \geqslant 3$) spectral lines of He-like oxygen, the wave function of an excited electron was approximated by the Coulomb wave functions. Taking into account the linear Stark shift in the ion microfield, the broadening by elastic electron-ion collisions, and the Doppler shift, the S_{n1} function has the form

$$S_{n1}(\omega) = \frac{1}{\sqrt{\pi}\gamma_{n1}^D g_n A_{n1}}$$

$$\times \sum_\alpha A_{n\alpha 1} \int_0^\infty V\left(\frac{\omega - \omega_{n1} - \Delta_{n\alpha}\beta}{\gamma_{n1}^D}, \frac{\gamma_{n\alpha 1}}{\gamma_{n1}^D}\right) P(a, Z_i, \beta)\mathrm{d}\beta, \qquad (5)$$

where $A_{n\alpha 1}$ is the rate of the $n\alpha(n_1, n_2, m) \to 1$ radiative transition for the sublevel with the parabolic quantum numbers n_1, n_1, and m; $A_{n1} = g_n^{-1} \sum_\alpha A_{n\alpha 1}$ is the same quantity for the level n as a whole; $V(x, y)$ is the Voigt contour with the Doppler width $\gamma_{n1}^D(T_i)$ and the collision width $\gamma_{n\alpha 1}(N_e, T_e)$ [18]; T_e and N_e are the electron temperature and density; $\Delta_{n\alpha}$ is the linear Stark shift of the sublevel induced by the ion field with the average intensity $F_0 = Z_i e/r_0^2; r_0 = 0.62 N_i^{-1/3}$ is the average distance between ions; Z_i and N_i

are the average charge and the density of ions; T_i is the effective ion temperature that takes the macroscopic plasma motion into account. The distribution function $P(a,Z_i,\beta)$ of the ion microfield $F = F_0\beta$ takes into account the ion correlation and the Debye screening [19], where the parameter $a = r_0/r_D$ is determined by the number of ions in a sphere with the Debye radius r_D. For $a \ll 1$, the function P transforms into the known Holtsmark distribution function [20].

The level population densities were calculated in the context of a collision-radiative model with the inclusion of the reabsorption of the resonance radiation in the Biberman–Holstein approximation [21]. The characteristics of bound-free and free-free transitions in expressions (2) and (3) were calculated from formulas given in Ref. [22]. The escape factors were taken from the calculations performed in Ref. [23].

Upon the expansion of dense, highly ionised species in the background medium (following the irradiation by a laser pulse), the typical relaxation times of the ionic excited states in the plasma are far shorter than the characteristic electron-density relaxation times, and therefore, the stationary sink approximation [24] was used to calculate the population densities. The ionic-charge plasma composition and T_e, L_i, and C_i, which corresponded to the given N_e, were determined by fitting the synthesised spectrum (1) to the results of measurements of the widths and the relative intensities of the lines observed. The validity of a multiparameter description of time-integrated plasma spectra was demonstrated earlier (see, e.g., Refs [25, 26]).

4. Results and discussion

Figs 1b–d show spectrograms and a pinhole camera image of the x-ray emission of a CO_2 target plasma. One can see from the intensity distributions of the Ly_α line of H-like oxygen ions and the He_β line of He-like oxygen ions (Figs 1b and 2b) that the emitting plasma region is spatially structured along the direction of laser pulse propagation. The structure may appear due to the nonuniformity of the cluster density distribution in the gas jet [15]. It should be remembered that, owing to a large optical plasma thickness for the Ly_α and He_β lines, the actual average dimension of the hot regions along the laser beam is smaller than the observed one $\Delta z \approx 0.4$ mm (Fig. 2b), for their centre distance of $\sim$ 0.4 mm. The observed average dimension Δx in the lateral direction is closer to the actual one owing to the plasma transparency for the He_γ and He_β lines and is equal to approximately 0.2 mm (Fig. 2a). The two-dimensional plasma image in the soft x-ray emission produced by the pinhole camera (Fig. 1d) also demonstrates a well-defined spatial structure in the form of two luminous, partly overlapping regions, which is explained by the observation at an acute angle relative to the laser beam.

Note that the observed line profiles are symmetrical. According to the results obtained earlier for CO_2 clusters at higher intensities of 60-fs laser pulses [13], this implies that fast ions, whose radiation gives rise to asymmetry of the line wings, are not produced in sufficient amounts under these conditions in the plasma.

Fig. 3 depicts the results of modelling of the emission spectra of H- and He-like oxygen ions in the CO_2 plasma. The excited-state population densities of oxygen ions and their charge-state distribution were calculated assuming that the fraction of Li-like ions is small and that carbon is

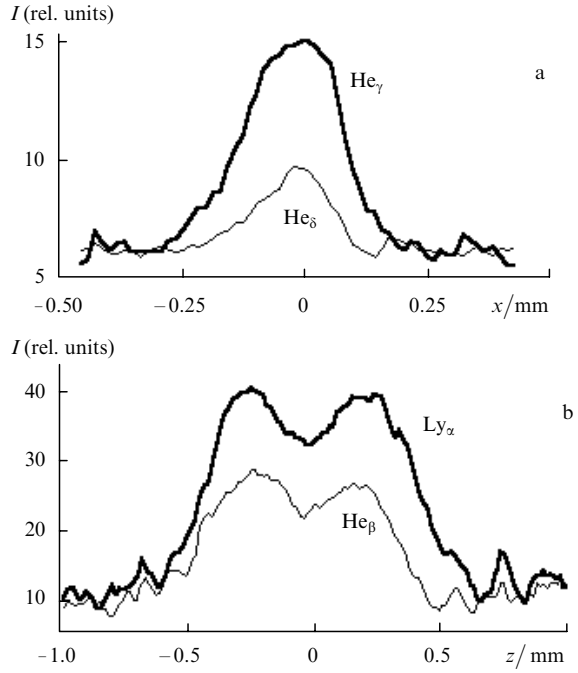

Figure 2. Spatial distribution of the intensity I of the CO_2-plasma emission at the line centres measured across (a) and along (b) the laser beam direction.

completely ionised. The observed spectrum was approximated by the sum of two terms in expression (1), which corresponded to the electron densities $N_{e1} = N_e^{cr}$ and $N_{e2} = 0.1N_e^{cr}$. This rough approximation is partly compensated by a reduction in the number of fitting parameters, which is significant in optimisation problems. As was found, stationary densities of oxygen ions of different multiplicity, which correspond to the chosen N_e values and the resultant T_e values, may be incorporated into the calculations. This allows us to employ the same C_i values for the Ly_α and He_β lines and thereby reduce the number of fitting parameters.

The Ly_α-to-He_β line intensity ratio depends strongly on the electron temperature via the excited-level population densities. By varying the temperature T_e and the parameter L_i for a fixed density $N_e = N_{e1}$, we fitted the level populations and the optical thickness for the lines in order to describe the wings of these lines (see Fig. 3). The centre of the lines was described by the contribution of the component with $N_e = N_{e2}$. The parameters C_1, C_2 and L_1, L_2 were controlled by the corresponding contributions to optically thin lines He_γ and He_δ, whose Stark profiles depended only slightly on the temperature. From expression (4) follows that the parameters C_i and L_i are not independent in this case. The fit yielded the following values: $T_{e1} = 115$ eV, $T_{e2} = 100$ eV, $L_1 = 100$ μm, $L_2 = 300$ μm. Instead of the effective ion temperatures T_{i1} and T_{i2}, which affect only the line centre, we used T_{e1} and 300 eV, respectively.

It is interesting to note that modelling the spectra that were obtained using two different spectrographs (*1* and *2* in Fig. 1a) required only a renormalisation of the corresponding parameters C_1 and C_2. A common normalising factor of 0.7 for the Ly_α and He_β lines relative to the He_γ and He_β lines (Fig. 3) is explained by the fact that only one of the two hot plasma regions contributes to the measured intensity of the latter two lines (owing to the spatial resolution of the spectro-

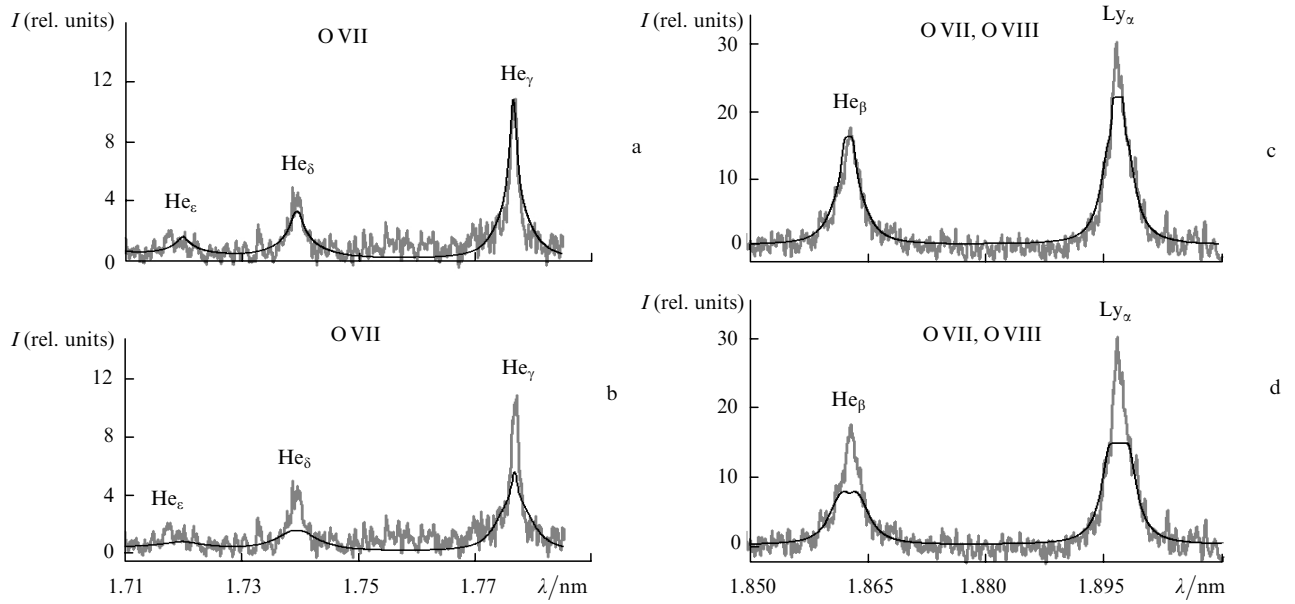

Figure 3. Comparison of the measured CO_2 plasma spectrum (the grey curves), corrected for the densitometer calibration curve, the sensitivity of the photographic film, and the filter absorption, with the results of model calculations (the black curves) for the $1s4p - 1s^2$ (He_γ),$1s5p - 1s^2$ (He_δ), and $1s6p - 1s^2$(He_ε) lines of O VII ions (spectrograph *2* in Fig. 1a) (a, b) and also for the Ly_α line of O VIII ions and the $1s3p - 1s^2$ (He_β) line of O VII ions (spectrograph *1* in Fig. 1a) (c, d). The calculations were performed for all the plasma components (a, c) and for components with the critical electron density (b, d).

graph). The results of modelling suggest that the main contribution to the time-integrated intensity of the Ly_α and He_β lines is made by the plasma with $N_e = N_e^{cr}$ (see Fig. 3b).

This result seems to be realistic, despite the apparent contradiction to the fact that the plasma was produced from clusters having a density far greater than the critical one. The typical radiative lifetimes of excited ion states are shorter than the cluster decomposition time ~1 ps. However, one should take into account that the radiation yield at this period is reduced owing to radiation reabsorption and the prevalence of inelastic nonradiative transitions in electron-ion collisions. A higher electron temperature also does not manifest itself in the spectra because it corresponds to the phase of ionisation at a high electron density. Simulations of the time evolution of the plasma parameters upon absorption of laser radiation in Xe clusters [27] suggest that the period of time during which $T_e > 300$ eV (i.e., exceeds 0.1 of the ionisation potential of Ni-like ions) is 0.2 ps, which is far shorter than the cluster decomposition time over which the temperature drops sharply down to 200 – 100 eV.

The contribution of high densities is manifested in the specific features of the x-ray emission spectrum of the plasma produced for the same laser pulse parameters in a Kr cluster target. Fig. 4 shows the results of measurements in the vicinity of the $(2s_{1/2}2p^6\,3p_{3/2})_1 - 2s^2\,2p^6\,{}^1S_0$ (peak *1*) and $(2s_{1/2}2p^6\,3p_{1/2})_1 - 2s^2 2p^6\,{}^1S_0$) (peak *2*) resonance lines of Ne-like KrXXVII ions. Since the ionisation energy of this ion $E_i \approx$ 2.9 keV is three times that of O VIII, the emission lines of a Ne-like Kr ion are observable only when the plasma electrons are strongly heated. The multiphoton mechanism of the x-ray emission on transitions in the *L*-shell of krypton, proposed in Ref. [14] to interpret the results obtained therein, presumably is inefficient in this case because the laser radiation is not intense enough and its wavelength is longer. The observed intensity ratios of the $3l3l' - 2p3l'$ and $3l4l' - 2p4l'$ dielectronic Na-like satellites to the corresponding resonance lines far exceed the ratios obtained in the experiments with nanosecond laser pulses [28], where a characteristic electron density of the order of 10^{20} cm^{-3} was established. Since the optical thickness of the plasma for satellite lines is small, their intensity, relative to the resonance lines, increases with increasing electron density.

5. Conclusions

Our study showed that the plasma produced by a femtosecond laser pulse in CO_2 and Kr gas targets exhibits the emission of highly charged ions. However, a maximum pulse intensity of 10^{17} W cm^{-2} is several orders of magni-

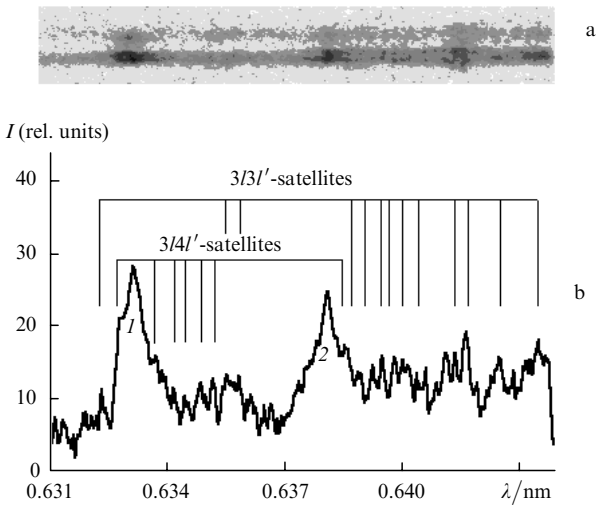

Figure 4. Spectrogram (a) and spectrum (b) of the $(2s_{1/2}2p^6 3p_{3/2})_1 - 2s^2\,2p^6\,{}^1S_0$ (*1*) and $(2s_{1/2}2p^6\,3p_{1/2})_1 - 2s^2 2p^6\,{}^1S_0$ (*2*) resonance lines of a Ne-like KrXXVI ion and their dielectronic satellites of Na-like ions recorded with spectrograph *1* (see Fig. 1a) in the third order of reflection.

tude lower than the threshold intensity for the tunnel ionisation of these ions in the laser field. The highly charged ions can appear when the electron temperature rises sharply owing to collision processes. The role of collision processes in the CO_2 and Kr gas jet targets under study is great because they result in the formation of clusters, whose density is close to that of solids. For a laser pulse length of 35 fs, the highly ionised plasma forms after the passage of the pulse.

The measured x-ray spectra show no characteristic evidence of fast-ion production unlike, for instance, the findings of Ref. [13]. The reason why the acceleration of ions by a Coulomb cluster explosion is inefficient may lie in the fact that the laser radiation intensity is not high enough to accomplish a spatial charge separation. The emission spectra in the O VII and O VIII ion resonance line series are adequately reproduced in the modelling using a quasi-stationary collision-radiative kinetic model with the inclusion of the principal mechanisms of broadening and absorption in a plasma having a high optical density.

The results suggest that the main contribution to the time-integrated spectrum is made by the plasma region with a near-critical electron density and a temperature of about 100 eV. The emission spectra of a krypton plasma in the vicinity of the resonance lines of Ne-like Kr ions were obtained for the first time when the tunnel ionisation and the multiphoton x-ray emission [14] are inefficient. This also points to the dominant role of collision cluster ionisation when the electron density and temperature are high. In this case, an increase in the relative intensity of the dielectronic satellites of resonance lines is observed. A rapid decrease of the temperature upon the decomposition of clusters provides the conditions for the inverse population of the levels of Ne-like ions and the realisation of an x-ray laser scheme.

References

1. Chang Z, Rundquist A, Wang H, et al. *Phys. Rev. Lett*. **79** 2967 (1997)
2. Borisov A B, Borovskiy A V, Shiryaev O B, et al. *Phys. Rev. A* **45** 5830 (1992)
3. Esaray E, Sprangle P, Krall J, Ting A IEEE *J. Quantum Electron*. **33** 1879 (1997)
4. Sarkisov G S, Bychenkov V Yu, Novikov V N, et al. *Phys. Rev. E: Stat. Phys., Plasmas, Fluids, Relat. Interdiscip. Top.* **59** 7042 (1999)
5. Monot P, Auguste T, Gibbon P, et al. *Phys. Rev. Lett*. **74** 2953 (1995)
6. Sakharov A S, Naumova N M, Bulanov S V *Plasma Phys. Rep.* **24** 818 (1998)
7. Burnett N H, Enright G D *IEEE J. Quantum Electron*. **26** 1797 (1990)
8. Rosmej F B, Faenov A Ya, Pikuz T A, et al. J. *Phys. B: At., Mol. Opt. Phys*. **32** L107 (1999)
9. MsPherson A, Luk T S, Thompson B D, et al. *Appl. Phys. B* **57** 337 (1993)
10. Ditmire T, Donnelly T, Rubenchik A M, et al. *Phys. Rev. A* **53** 3379 (1996)
11. Lezius M, Dobosz S, Normand D, Schmidt M *Phys. Rev. Lett*. **80** 261 (1998)
12. Ditmire T, Zwelback J, Yanovsky V P, et al. *Nature* **398** 489 (1999)
13. Dobosz S, Schmidt M, Perdrix M, et al. *Zh. Eksp. Teor. Fiz.* **115** 2051 (1999) [*J. Exp. Theor. Phys*. **88** (6) 1122 (1999)]
14. MsPherson A, Luk T S, Thompson B D, et al. *Phys. Rev. Lett.* **72** 1810 (1994)
15. Stenz C, Blasco F (private communication)
16. Ammosov M V, Delone N B, Krainov V P *Zh. Eksp. Teor. Fiz*. **91** 2008 (1986)
17. Skobelev I Yu, Faenov A Ya, Bryunetkin B A, et al. *Zh. Eksp. Teor. Fiz*. **108** 1263 (1995) [*J. Exp. Theor. Phys*. **81** (4) 692 (1995)]
18. Griem H R *Spectral Line Broadening by Plasmas* (New York: Academic Press, 1974)
19. Tighe R J, Hooper C F, Jr *Phys. Rev. A* **14** 1514 (1976)
20. Holtsmark J *Ann. Phys*. **58** 577 (1919)
21. Biberman L M *Zh. Eksp. Teor. Fiz*. **17** 416 (1947); Holstein T *Phys. Rev*. **72** 1212 (1947)
22. Kogan V I, Migdal A B *Fizika Plazmy i Problema Upravlyaemykh Termoyadernykh Reaktsii* (Plasma Physics and Thermonuclear Research) Vol. 1 (Moscow: USSR Academy of Sciences, 1958) p. 172; Kogan V I, ibid. Vol. 3 (Moscow: USSR Academy of Sciences, 1958) p. 99
23. Borovskii A V, Bunkin F V, Derzhiev V I, et el. *Preprint No. 189* (Moscow: P N Lebedev Physics Institute, USSR Academy of Sciences, 1983)
24. Gudzenko L I, Yakovlenko S I *Plazmennye Lazery* (Plasma Lasers) (Moscow: Atomizdat, 1978) p. 49
25. Magunov A I, Skobelev I Yu, Faenov A Ya, et al. *Zh. Eksp. Teor. Fiz.* **108** 1625 (1995) [*J. Exp. Theor. Phys*. **81** (5) 891 (1995)]
26. Magunov A I, Faenov A Ya, Skobelev I Yu, et al. *Phys. Scr.* **55** 478 (1997)
27. Ditmire T, Patel P K, Smith R A, et al. *J. Phys. B: At., Mol. Opt. Phys.* **31** 2825 (1998)
28. Khakhalin S Ya, Dyakin V M, Faenov A Ya, et al. *J. Opt. Soc. Am. B: Opt. Phys*. **12** 1203 (1995)